

Stalagmite growth perturbations from the Kumaun Himalaya as potential earthquake recorders

C. P. Rajendran · Jaishri Sanwal · Kristin D. Morell ·
Mike Sandiford · B. S. Kotlia · John Hellstrom ·
Kusala Rajendran

Received: 17 November 2014 / Accepted: 1 December 2015 / Published online: 12 December 2015
© Springer Science+Business Media Dordrecht 2015

Abstract The central part of the Himalaya (Kumaun and Garhwal Provinces of India) is noted for its prolonged seismic quiescence, and therefore, developing a longer-term time series of past earthquakes to understand their recurrence pattern in this segment assumes importance. In addition to direct observations of offsets in stratigraphic exposures or other proxies like paleoliquefaction, deformation preserved within stalagmites (speleothems) in karst system can be analyzed to obtain continuous millennial scale time series of earthquakes. The Central Indian Himalaya hosts natural caves between major active thrusts forming potential storehouses for paleoseismological records. Here, we present results from the limestone caves in the Kumaun Himalaya and discuss the implications of

growth perturbations identified in the stalagmites as possible earthquake recorders. This article focuses on three stalagmites from the Dharamjali Cave located in the eastern Kumaun Himalaya, although two other caves, one of them located in the foothills, were also examined for their suitability. The growth anomalies in stalagmites include abrupt tilting or rotation of growth axes, growth termination, and breakage followed by regrowth. The U-Th age data from three specimens allow us to constrain the intervals of growth anomalies, and these were dated at 4273 ± 410 years BP (2673–1853 BC), 2782 ± 79 years BP (851–693 BC), 2498 ± 117 years BP (605–371 BC), 1503 ± 245 years BP (262–752 AD), 1346 ± 101 years BP (563–765 AD), and 687 ± 147 years BP (1176–1470 AD). The dates may correspond to the timings of major/great earthquakes in the region and the youngest event (1176–1470 AD) shows chronological correspondence with either one of the great medieval earthquakes (1050–1250 and 1259–1433 AD) evident from trench excavations across the Himalayan Frontal Thrust.

C. P. Rajendran · J. Sanwal (✉)
Geodynamics Unit, Jawaharlal Nehru Centre for Advanced Scientific Research, Bangalore 560064, India
e-mail: jaishrigeology@gmail.com

K. D. Morell · M. Sandiford · J. Hellstrom
School of Earth Sciences, University of Melbourne, Melbourne, VIC 3010, Australia

K. D. Morell
School of Earth and Ocean Sciences, University of Victoria, Victoria, BC, Canada

B. S. Kotlia
Centre of Advanced Study in Geology, Kumaun University, Nainital 263002, India

K. Rajendran
Centre for Earth Sciences, Indian Institute of Science, Bangalore 560012, India

Keywords Stalagmites · Speleoseismology · Earthquake recurrence · Central Indian Himalaya · Seismic gap

1 Introduction

Speleoseismological investigations conducted in some karst-dominated terrains have been able to identify earthquake-related damage and to develop chronologies

of those events (Kagan et al. 2005; Šebela 2008; Panno et al. 2009; Braun et al. 2011). The Himalayan mountain chain, at the interface of the India and Eurasia plates, recognized for its high seismic productivity and major/great earthquakes, offers a testable ground for the application of this approach. Located between the rupture zones of the 1905 and 1934 earthquakes (Fig. 1a), the Kumaun-Garhwal Himalaya, along with western Nepal, represents a segment, known as the “central seismic gap” (Khattri 1987). The recent April–May Nepal earthquakes occurred toward the eastern extremity of the central seismic gap (Parameswaran et al. 2015). Another significant earthquake in the region occurred in 1803 ($M_w \sim 7.5$), close to the town of Uttarkashi (Fig. 1a) on the western part of the seismic gap (Rajendran et al. 2013). The historical and geological evidence suggests the occurrences of major earthquakes within the central Himalayan seismic gap from Early to Late Middle Ages (Ambraseys and Jackson 2003; Bilham and Ambraseys 2005; Kumar et al. 2006, 2010; Rajendran and Rajendran 2011; Rajendran et al. 2013, 2015). Interpretations of the trench sections excavated in the central Himalaya along the Himalayan Frontal Thrust (HFT) (Kumar et al. 2006) indicate an event that occurred between 1258 and 1423 AD (Fig. 1a). The observations from a trench in central Nepal (Fig. 1a), east of the Kathmandu *klippe*, suggest a great earthquake in 1255 AD (Sapkota et al. 2013). Recent fault excavations on the HFT in central Himalaya (Fig. 1a) suggest at least two great earthquakes in the central Himalaya between 1259–1433 and 1050–1250 AD (Rajendran et al. 2015). These estimates of earthquake recurrences in this region, in general, do not go beyond one or two previous generations of faulting as the observations are limited by the shallow exposure depth in trenches.

Aside from the great décollement earthquakes that may rupture the HFT, studies in the central Himalaya also posit an active thrust fault or duplex, located nearly 100 km north of the HFT (Wobus et al. 2006; Morell et al. 2015). A dense zone of seismicity is associated with this zone and is related to the mid-crustal ramp in the Main Himalayan Thrust (MHT) (Ni and Barazangi 1984; Pandey et al. 1995; Mahesh et al. 2013). The major earthquake of 1803 ($M_w \sim 7.5$) near Uttarkashi, for example, might have occurred within this zone (Rajendran et al. 2013). The recent April ($M_w 7.8$) Nepal earthquake (Fig. 1a, for location) underscores the role of out-of-sequence thrusts in accommodating

seismic slip (Parameswaran et al. 2015). It is possible that some of these earthquakes may be associated with blind thrusts. Even if the surface faulting had occurred, the poorly preserved exposures and thick vegetation could hinder its identification. In such situations, particularly in the regions where caves are accessible, the use of stalagmite deformations as proxy for constraining the timing of causative earthquakes can circumvent the issues relating to poor or shallow fault exposures and lack of surface ruptures. Another advantage is that the U/Th dating applied to speleoseismites help in extending the time window of deformation beyond the resolving capability of radiocarbon dating (40 ka)—an often used dating technique in trenches. The U/Th method provides a high temporal resolution going back in time up to 500 ka (Vaks et al. 2013).

Limestone caves in the Himalaya are mostly distributed between the Main Central Thrust (MCT) and the Main Boundary Thrust (MBT) (Fig. 1a, b). Therefore, speleoseismite studies are helpful to understand the seismic activities associated with hinterland structures (e.g., the MCT and MBT or any other less prominent thrusts), in lieu of great décollement earthquakes that rupture the HFT. Here, we explore the usefulness of the growth deformations preserved in stalagmites from three caves in the central Himalaya (Fig. 1a, b), as proxies for timings associated with earthquake-driven deformations.

2 Background and Previous Studies

Speleothems include a variety of cave formations such as stalagmites, stalactites, soda straws, flowstones, and draperies. Among these, stalagmites are considered as the most potential archives of climatic signals. Further, the speleothems usually act as closed system with respect to U-series isotopes and are ideal to establish the absolute chronology (Atkinson et al. 1978; Baker et al. 1993b; Shopov et al. 1994; Musgrove et al. 2001; Vaks et al. 2006; Shen et al. 2012; Gopher et al. 2010). Much of the previous speleological studies focused on the growth history of stalagmites to understand the paleoclimatic variables (Dorale et al. 1998; Baker et al. 1993a; Fleitmann et al. 2004; Treble et al. 2005; Banner et al. 2007; Holzkämper et al. 2009; Fairchild and Baker 2012; Mariethoz et al. 2012; Orlanda et al. 2012; Railsback et al. 2013; Shen et al. 2013).

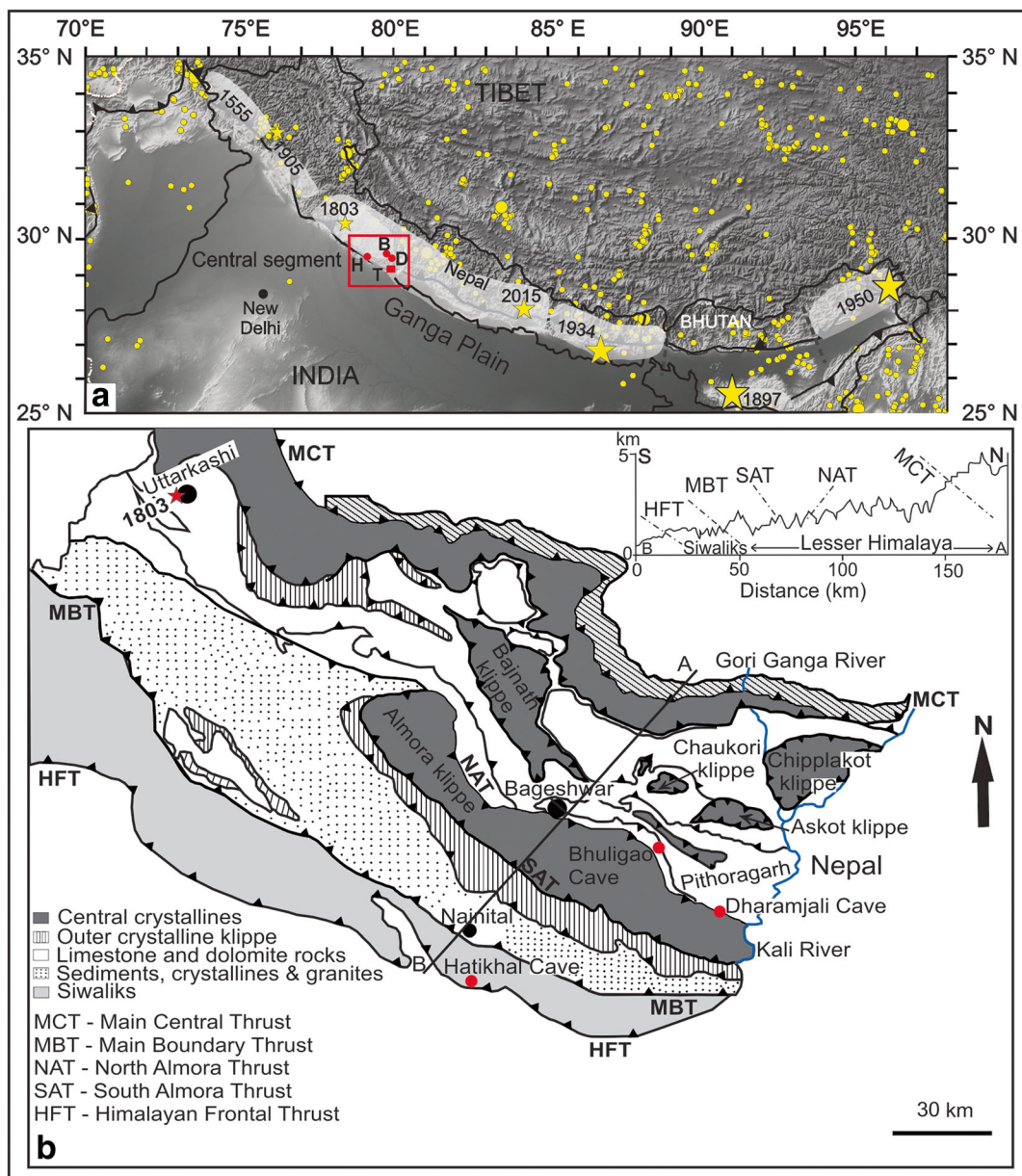


Fig. 1 **a** A map showing historical earthquakes (yellow stars) along the Himalayan arc (Rajendran et al. 2015) and the regional seismicity (yellow filled circles). The location of the April 25 Nepal Earthquake is also shown. The study area is demarcated

by a square: *B*, Bhuligao Cave; *D*, Dharamjali Cave; *H*, Hathikhal Cave. Trench locations on the Himalayan frontal thrust are shown by filled red rectangles. **b** Geological map and cross section of the study area (modified after Valdiya 1980) with locations of caves

In addition to elucidating climate signals, recent global examples suggest that the deformation of speleothems can be used as a proxy for earthquake-related ground shaking (Cadorin et al. 2001; Forti 2001; Becker et al. 2006; Kagan et al. 2005; 2006; Šebela 2008; Panno et al. 2009). Because the width and length of the stalagmite depend on the drip water,

the size of the droplet and the distance from the ceiling, each layer preserved within the stalagmite often acts as a repository of its growth history. As stalagmites grow upward from the cave floor, receiving water droplets of dissolved calcium carbonate from the roof, any change in the orientation or alignment with the roof is likely to affect the vertical growth axis pattern in the

stalagmite. The shifts in orientations may also be attributed to earthquake shaking and consequent ground level changes. Deciphering tectonic imprints preserved within speleothems, therefore, involves identifying growth deformations (e.g., changes in the orientation of growth axis or breakages) and bracketing their ages. The use of speleothems as paleoseismic indicators is widely discussed by several workers (Forti and Postpischl 1984; Postpischl et al. 1991; Lemeille et al. 1999; Gilli 1999, 2004, 2005; Delaby 2001; Becker et al. 2006; Šebela 2008).

The studies suggest that roof collapse in caves may have a causal link with earthquake-related shaking, the effects of which could manifest in different ways. For example, rock falls triggered by earthquakes could damage speleothems and those fragments together with rock fall blocks may rest on the cave floor as debris on which juvenile ones grow (Kagan et al. 2005; Becker et al. 2006). It is equally possible that the stalagmite (speleothem) breakages happen due to nontectonic processes like sliding of the cave floor and water wash or landslides (Forti 2001). In a study of speleothems of Soreq Cave, located within the Dead Sea Transform region, Kagan et al. (2005) were able to link the fallen cave ceilings to earthquakes, and U-Th dates of the event are concurrent with broken stalactites and stalagmites from other parts of the cave. The simultaneity of deformational events like ceiling collapses and speleothem breakages thus can be used as a criterion to establish the seismogenic nature of deformation within the caves. Structural interpretations of growth deformations within the stalagmites combined with chronology of the deformational phases are also used in these studies to resolve earthquake history. Such approaches have been followed successfully to identify pre-historical earthquakes in locations like the Dead Sea transform and the mid-western region of the United States (Kagan et al. 2005; Panno et al. 2009; Braun et al. 2011).

In the Indian Himalaya, well-preserved and long-lived cave deposits have been subjected to extensive paleoclimatic studies (Sinha et al. 2005; Kotlia et al. 2012, 2014; Duan et al. 2013; Sanwal et al. 2013). But, till date, no paleoseismite study has been attempted in the Himalaya despite the fact that the region hosts numerous limestone caves. The study presented here is first of its kind from this region. We investigated three caves in the Kumaun Himalaya, the first two caves situated between the MCT and the MBT (Figs. 1a, b and 2a–g) the third at the HFT (Figs. 1a, b and 3d, f)

during different field campaigns (November 2010 to November 2012). Our speleoseismite investigations included examination of the speleothems for any kind of growth perturbations, tilting, or other features that reveal structural damages to the caves including collapse of ceilings. In order to avoid any random destruction to cave environment, the sample collections were done only after ascertaining the usefulness and scope of samples for further analyses. The ages of various layers within the samples were obtained by U-Th series analysis.

3 Study Sites

We explored three caves in the Kumaun central Himalaya, of which two caves Dharamjali ($29^{\circ} 31' 27.8''$ N, $80^{\circ} 12' 40.3''$ E) and Bhuligao ($29^{\circ} 36' 53.6''$ N, $80^{\circ} 04' 45.9''$ E), are located in the Pithoragarh District in eastern Kumaun Himalaya. The third cave, Hathikhal ($29^{\circ} 19' 01.5''$ N, $79^{\circ} 25' 49.8''$ E) is located in the foothills of sub-Himalaya near Nainital (Fig. 1b). The Dharamjali Cave, the main focus of this study, is formed in the Precambrian Thalkedar limestone (the Mandhali Formation of Tejam Group of rocks, after Valdiya 1980). The Bhuligao Cave is situated ~10 km from Gangolihat, which is ~75 km NW of Pithoragarh Town. The Bhuligao Cave is formed in the Gangolihat limestone (Deoban Formation of Tejam Group of rocks, after Valdiya 1980) at an elevation of 1405 m. Hathikhal Cave is situated ~17 km south of Nainital within the Siwalik Formation at an elevation of ~805 m within the foot of the Himalaya. Carbonate source for this cave may not be the rock sequences located far (~20 km) to the north. Rather, it is more likely that the occasional calcareous band embedded in the host sandstone of the Middle Siwalik Formation itself may have acted as the source (Valdiya 2010).

Both the Dharamjali and Bhuligao Caves are situated on the top of a hill and exhibited any evidence of recent landslides or water wash in the vicinity. The Hathikhal Cave is located close to a small stream but the morphology around the cave showed no indications of any landslide. Our focus was to identify the growth perturbations on the speleothems, roof collapses, and deposition of debris inside the caves. The Dharamjali Cave exhibited tilted stalagmites, toppled older-generation stalagmites, and showed evidence for regrowth of juveniles, as well as multiple generations of ceiling collapse

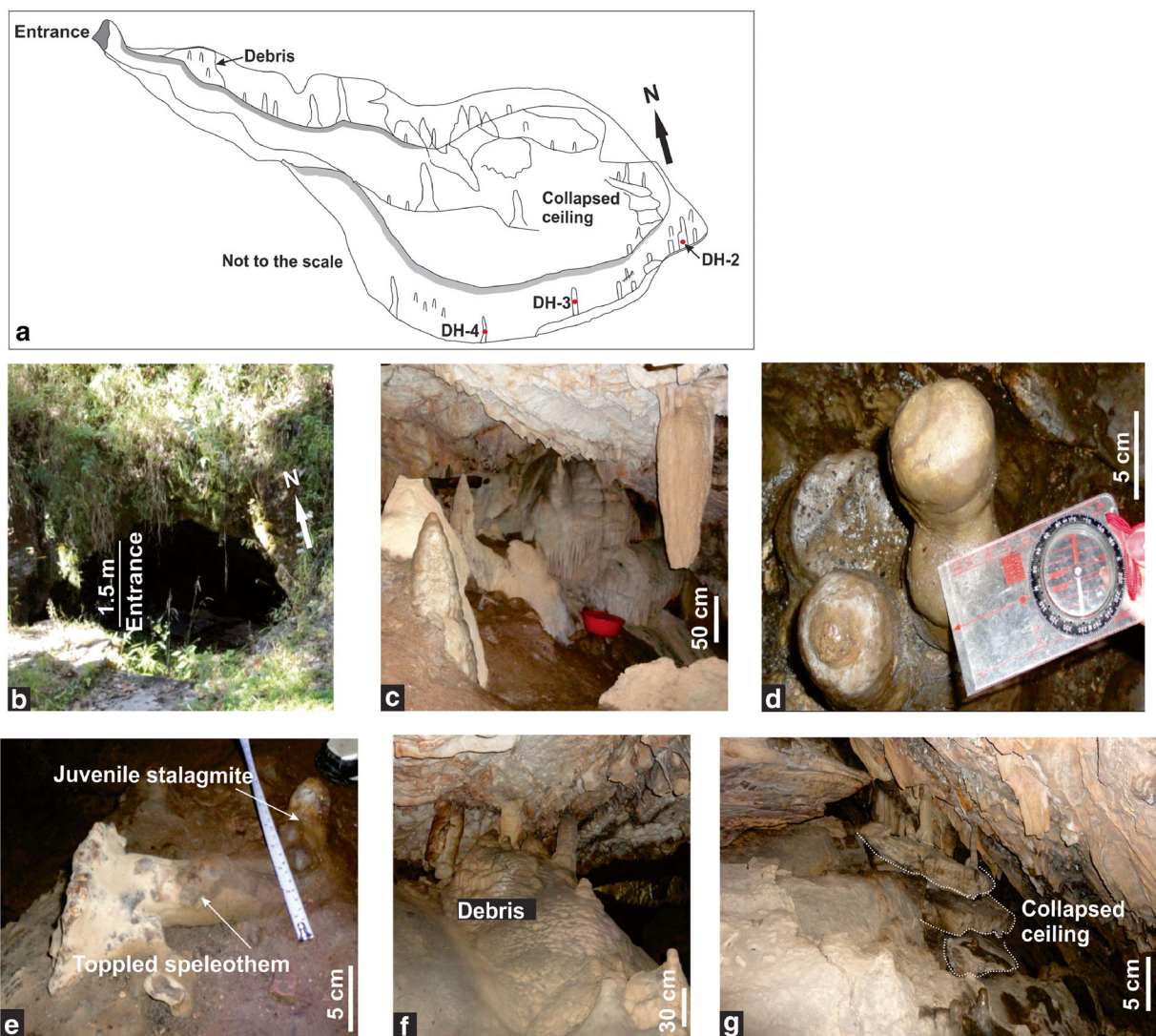


Fig. 2 **a** A sketch of Dharamjali Cave. **b**, **c** Entrance of Dharamjali Cave. **c** Interior of Dharamjali Cave. **d** Sample DH-2 in *in situ* position (Dharamjali Cave). **e** Growth of juvenile stalagmite on a toppled speleothem (Dharamjali Cave). **f** An earlier surface

formed by debris of speleothems with juvenile stalagmites (Dharamjali Cave). **g** Sets of collapsed ceiling with the growth of juvenile stalagmites (Dharamjali Cave)

(Fig. 2e–g). The Bhuligao Cave featured a large number of speleothems growing not only on the host rock but also on the 1–1.5-m-thick debris of inactive broken speleothems (Fig. 3a–c). The debris of damaged speleothems is interpreted to have been formed by earthquake shaking given that no other possible reasons or evidence can be ascribed to explain this damage. The Hathikhal Cave, located close to the HFT comprises a narrow passage (~1 m wide and ~2 m long, see Fig. 3d) and a distinct chamber. The cave showed no indication of broken speleothems or any related debris (Fig. 3e) that by itself may not be taken as a proof for absence of

seismic shaking in cave's history. The stalagmite growth in the cave was restricted to the 25° northwest dipping side wall (Fig. 3e). Two samples from this cave (1 and 2 in Fig. 3e, f) showed clear indications of periodic tilts in the opposite direction of slope of the wall (Fig. 3e, f). These remarkable tilts in the growth axes may be potentially relevant to earthquake-related deformations that must have occurred on the HFT.

All three caves exhibited deformed stalagmites, but the chronological constraints on deformational events in of this study are exclusively based on dates obtained from samples within the Dharamjali Cave. Therefore,

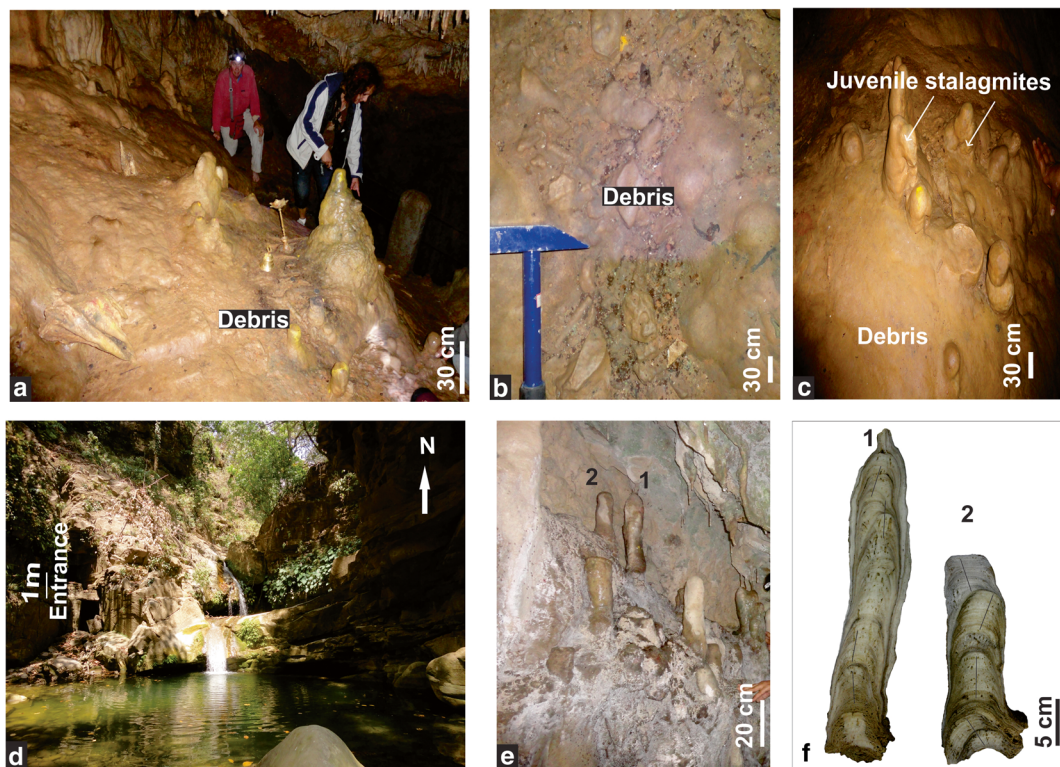


Fig. 3 **a** Interior of Bhuligao Cave showing debris of speleothems. **b** Cave floor with speleothem debris (Bhuligao Cave). **c** Growth of juveniles on an earlier surface of speleothem debris (Bhuligao Cave). **d** Entrance of Hathikhal Cave; **e** Interior

of Hathikhal Cave showing in situ growth position of two specimens. **f** Polished vertical sections of stalagmites (**1** and **2**) recovered from Hathikhal Cave (note the tilts in growth axes in both samples)

here, we focus on the samples from the Dharamjali Cave in order to develop a longer-term time series of great earthquakes in the central Indian Himalaya owing to its location within an actively deforming area close to the MCT (Fig. 1b). Furthermore, the age data from the Dharamjali Cave had the minimum error, whereas the stalagmites from the Bhuligao and Hathikhal Caves displayed large error in U/Th dating due to the excess thorium contamination. Therefore, the dates obtained on the stalagmites from the latter caves are not used in the present study. We, however, emphasize that further studies are required to make a final assessment on the suitability of the samples for dating from the Bhuligao and Hathikhal Caves. In the next section, we present the features of the Dharamjali Cave that underpin the major conclusions of our study.

3.1 The Dharamjali Cave

The Dharamjali Cave, located ~15 km southwest of Pithoragarh, sits at an elevation of 2210 m, west of the

Kali River (Fig. 1b). This site occurs above a ramp in the MHT and is bounded by the MCT, ~50 km to the north, and the MBT, ~40 km to the south (Fig. 1a, b). Another important structure in the region is the north-dipping “North Almora Thrust” (NAT) that occurs to the south, and being a part of a nappe the NAT may not be an active structure (Célérier et al. 2009; Fig. 1b). The rocks of the area consist of both crystalline and sedimentary sequences, and structurally, they form the Almora nappe. The massive limestones that are calcitic in composition and interbedded with dolomites (Valdiya 1980) form the host rock for the development of caves in the region. The 35-m-long subvertical cave consists of a wider first chamber (30 m long and 3 m wide) and a narrow second chamber (0.8–0.9 m in width) (Sanwal et al. 2013). The cave exhibits abundant and well-developed stalagmites, stalactites, and soda straws. Many of these stalagmites are currently in a stage of active growth and a few can be categorized as juveniles, and some with post-damage regrowths on broken speleothems. The cave is mostly wet throughout the

year and expectedly the drip water percolation increases during the rainy season (20–30 drops/min) (Sanwal et al. 2013). The cave floor also shows signs of fallen blocks of the roof, upon which young stalagmites are growing.

As indicated earlier, caves with wide entrances are not well suited for U-Th analyses as the speleothems are likely to get excessively exposed to wind-borne particles that include thorium in them. It is also possible that detrital thorium is contributed also by drip water that percolates through the soil. The Dharamjali Cave has a narrow passage (~1 m) and forms an ideal setting as it is insulated from external ambient influences. Considering the fact that the humidity is as high as 70–75 % for a cave that has a small entrance, the kinetic fractionation may be negligible, which controls the equilibrium conditions. Following the same reasoning, it is also essential to ensure that no external factors, including human interference have affected the natural growth of the speleothems. This aspect is particularly relevant to the caves in the Himalaya as many of them are used for religious and ritualistic purposes. The Dharamjali Cave showed no such indications, except occasional human occupation close to the entrance. All the samples for this study were collected far inside the cave where wind-borne contamination and human interference are expected to be least (Fig. 2a).

4 Methods

Here, we focus on three stalagmites from the Dharamjali Cave that show a change in growth axis: DH-2 (length 17.5 cm; width 5–8 cm), DH-3 (length 16 cm; width 4–5 cm), and DH-4 (length 20 cm; width 3–5 cm). Two stalagmites DH-2 and DH-4 were actively receiving the drip water from the roof prior to sampling, whereas DH-3 was inactive. The first two samples (DH-2 and DH-3) were collected from the lower second chamber, ~33 m from the cave entrance, while the third (DH-4) was collected from the first chamber, ~20 m from the cave entrance. After recording the tilt of the stalagmites, we cut them at their base. The samples were sliced in the laboratory along their axial planes to obtain vertical sections and were then polished in order to conduct detailed examination of their morphology and preserved growth features. Deformational horizons defined by abrupt tilting or rotation of growth axes or growth

termination, breakage, and regrowth were identified for further visual and microscopic examination.

The stalagmite depths for the age sampling were measured as a series of line segments that pass through the thickest part of each growth horizon, and in this way, the cumulative depth considerably exceeds the apparent length of the stalagmite. Specimens were microsampled for U-Th dating along their growth axes using a modified dental drill consisting of a 1-mm drill bit. Powdered samples weighing about 200 mg that were chosen to bracket the deformation event from above and below were collected. Although we have bracketed ages across growth perturbations as closely as possible, the selection of age sampling areas were dictated primarily by the condition whether the area affected by impurities or secondary contamination that needs to be avoided. These ideal locations on the samples were identified *prima facie* by visual observation. U and Th were measured on a multicollector-inductively coupled plasma mass spectrometer at the Melbourne University, Australia (Table 1). The U and Th isotope ratios were determined simultaneously using the parallel ion counting technique, as followed in Hellstrom (2003). As the samples were in actively growing phase, we estimated calendar years with the age of the top end as 2010 AD, the year of sample collection.

As mentioned earlier, some stalagmite specimens may not be uniformly useful for dating because of localized thorium contamination within their growth bands. Thus, a primary requirement for U/Th dating is the “cleanliness” of sampling locations within stalagmite specimens. Therefore, in some instances, the sampled areas on the stalagmite specimens for age determinations may not overlap the areas showing growth disturbance. In such cases, we relied on interpolating the timings of deformation from closest adjacent available U-series dates by utilizing the distance between growth deformations along the axis. U-Th ages were calculated for all samples using Eq. 1 of Hellstrom (2006), which corrects for initial Th, with the ^{234}U and ^{230}Th half-lives of Cheng et al. (2013). The most probable initial $^{230}\text{Th}/^{232}\text{Th}$ activity ratio of 0.43 ± 0.08 was determined using stratigraphic constraint of stalagmites DH-2 and DH-3 (e.g., Hellstrom 2006).

All three stalagmites (DH-2, DH-3, and DH-4) from the Dharamjali Cave showed indications of disturbances along their growth trajectory. We have arrived at the interpolated dates of the growth anomalies in these samples using the StalAge age model, developed by

Table 1 U/Th dates of stalagmite samples (DH-2, DH-3 and DH-4) from the Dharamjali Cave, central Himalaya

Sample	Apparent depth from the top (cm)	Mass/g	$U(\text{ngg}^{-1})$ $(^{238}\text{U}/\text{ng/g})$	$[^{230}\text{Th}/^{238}\text{U}]^a$	$[^{234}\text{U}/^{238}\text{U}]^a$	$[^{234}\text{U}/^{238}\text{U}]_j^c$	$[^{232}\text{Th}/^{238}\text{U}]$	$[^{230}\text{Th}/^{232}\text{Th}]$	Age(ka) ^b
DH-2									
MS-05	1.1	0.15	219	0.00573±.00027	1.7478±.0035	1.7482±.0035	0.006149±.000057	0.9	0.191±.036
MS-30	1.3	0.08	273	0.00478±.00035	1.7464±.0044	1.7469±.0044	0.001924±.000009	2.5	0.249±.021
MS-29	4.6	0.10	340	0.00748±.00037	1.7481±.0045	1.7490±.0045	0.001015±.000006	7.4	0.442±.026
MS-04	5.8	0.09	443	0.00766±.00018	1.7454±.0034	1.7464±.0034	0.000715±.000009	10.7	0.463±.013
MS-34	6.7	0.09	331	0.01242±.00071	1.7460±.0043	1.7472±.0043	0.007432±.000119	1.7	0.577±.058
MS-03	9.5	0.14	295	0.01785±.00048	1.7146±.0033	1.7167±.0033	0.003784±.000097	4.7	1.040±.038
MS-33	9.8	0.14	255	0.01947±.00049	1.7134±.0044	1.7156±.0044	0.006588±.000042	3.0	1.067±.047
MS-32	17.0	0.21	1008	0.02351±.00021	1.6659±.0043	1.6689±.0043	0.000666±.000001	357.6	1.546±.014
MS-02	21.2	0.19	986	0.0264±.00037	1.6522±.0032	1.6550±.0032	0.000152±.000002	173.4	1.751±.027
MS-31	23.1	0.07	737	0.02833±.00026	1.6357±.0045	1.6390±.0045	0.002672±.000024	10.6	1.825±.025
MS-1	25.2	0.14	61	0.0374±.00061	1.6320±.0040	1.6358±.0040	0.014968±.000104	2.5	2.095±.091
DH-3									
MS-28	0.7	0.10	2415	0.02989±.00019	1.5527±.0039	1.5560±.0039	0.000317±.000002	94.4	2.108±.015
MS-24	1.2	0.07	135	0.03213±.00267	1.5415±.0088	1.5448±.0088	0.004840±.000035	6.6	2.145±.198
MS-27	2.8	0.10	771	0.03687±.00033	1.5103±.0039	1.5142±.0039	0.001015±.000005	36.3	2.662±.024
MS-25	2.3	0.09	205	0.04030±.00421	1.4913±.0062	1.4940±.0059	0.009365±.000038	4.3	2.691±.063
MS-26	7.0	0.07	1251	0.03830±.00039	1.5003±.0040	1.5042±.0040	0.001271±.000008	30.1	2.777±.032
MS-23	8.2	0.12	142	0.04022±.00261	1.4911±.0074	1.4950±.0074	0.005077±.002007	7.9	2.819±.197
DH-4									
MS-22 ^d	6.7	0.06	1902	0.0209±.0028	1.3302±.00668	1.3319±.00669	0.006426±.000040	3.3	1.503±.245
MS-20	22.7	0.07	4029	0.0442±.0010	1.2475±.0029	1.2491±.0336	0.000328±.000008	134.5	3.921±.145

Analytical errors are 2σ uncertainties in the last significant number^a Activity ratios determined after Hellstrom (2003)^b Age in kyr before present corrected for initial ^{230}Th using Equation 1 of Hellstrom (2006), $[^{230}\text{Th}/^{232}\text{Th}]_j$ of 0.43 ± 0.08 and the decay constants of Cheng et al. (2013)^c Initial $[^{234}\text{U}/^{238}\text{U}]$ is calculated using corrected age^d The large error in sample MS-22 could be the result of high uranium content in the sample

Scholz and Hoffmann (2011). A comparative discussion of the various available programs of linear interpolation of age data is given in Scholz et al. (2012). It is suggested that the StalAge algorithm is sensitive to the variation in the growth rate of the stalagmites and detects and corrects for data outliers and age inversions without overestimating the true variability in growth rate (see Scholz et al. 2012). Using this method, we also calculated corresponding 95 % confidence limits by Monte Carlo simulation (Scholz and Hoffmann 2011). Interpolated ages of growth anomalies (deformation events) of the stalagmites are presented in Table 2.

5 Analyses and results

The stalagmite specimen DH-2 generally shows an overall shift in its growth axis by 6° toward the northeast at ~7.36 cm from the top end of the specimen (Fig. 4). This specimen also shows a major shift of ~15° in its growth axis at a depth of ~13.5 cm. The interpolated dates obtained for these levels are 687±147 years BP (1176–1470 AD) and 1346±101 years BP (563–765 AD), respectively (Fig. 4; Table 2).

Stalagmite DH-3 shows signs of breakage at the uppermost part of the sample (at a depth of 1.5 cm) and subsequent regrowth after breakage (Fig. 4). The interpolated age of this breakage is 2498±117 years BP (605–371 BC). DH-3 also shows a minor tilting (~3°) of the growth axis in a northeast direction at about 6.9 cm from the top end of the specimen and is dated as 2782±79 years BP (851–693 BC) (Fig. 4; Table 2).

The sample DH-4 has preserved an embedded broken soda straw within the growth layers at a depth of 7.8 cm (Fig. 4; Table 2). We presume that the soda straw growing downward from the roof obstructed the upward growth of this stalagmite. The breakage of soda straw probably marks a major deformation event. The U-Th date of 1503±245 years BP (262–752 AD) obtained from the broken soda straw within the stalagmite at the breakage point is considered here as the age of this particular event (Fig. 4). This event noted in DH-4 is represented in DH-2 by an abrupt transition from lighter colored growth bands to darker shade (reflective of a change in the chemistry of drip water), which is dated at about the same period (1546±014 years BP) although no rotation of growth axis can be discerned. DH-4 also exhibits a tilt in growth axis at a lower level at ~23.5 cm, and the age is interpolated at 4273±410 years BP (2673–1853 BC) (Fig. 4).

All three stalagmites (DH-2, DH-3 and DH-4) fall in different age brackets and are expected to show variability in growth rate. Using the StalAge program, we estimated that the growth rate of the stalagmites (DH-2 and DH-3) varies from 45–170 and 0–110 μm/year, respectively (Fig. 5). The DH-3 shows a growth hiatus at the breakage marked at ~2 cm from the top (Figs. 4 and 5). This interval of hiatus may add a minor uncertainty in the age calibration and growth estimation for DH-3. However, the growth rate for DH-4 cannot be estimated because of the limited age data. Further the upward growth of this stalagmite appears to have been hindered toward the top by the breakage. As for DH-2, we could obtain more dense dating results, more or less

Table 2 Growth layer deformations and interpolated ages of event horizons in stalagmite samples (DH-2, DH-3 and DH-4; Fig. 4) from Dharamjali Cave

Apparent depth from the top (cm)	Growth layer deformations	Interpolated ages
DH-2		
7.36	The central growth axis has shifted about 3 cm from its original drip position.	687±147 years BP (1176–1470 AD)
13.5	Minor shift (2°) in growth axis.	1346±101 years BP (563–765 AD)
DH-3		
1.5	Breakage	2498±117 years BP (605–371 BC)
6.9	Tilt in growth axis (3° NE)	2782±79 years BP (851–693 BC)
DH-4		
7.8	Breakage and the remnant broken stalactite	1540±275 years BP (195–745 AD)
	Tilt in growth axis	4273±410 years BP (2673–1853 BC)

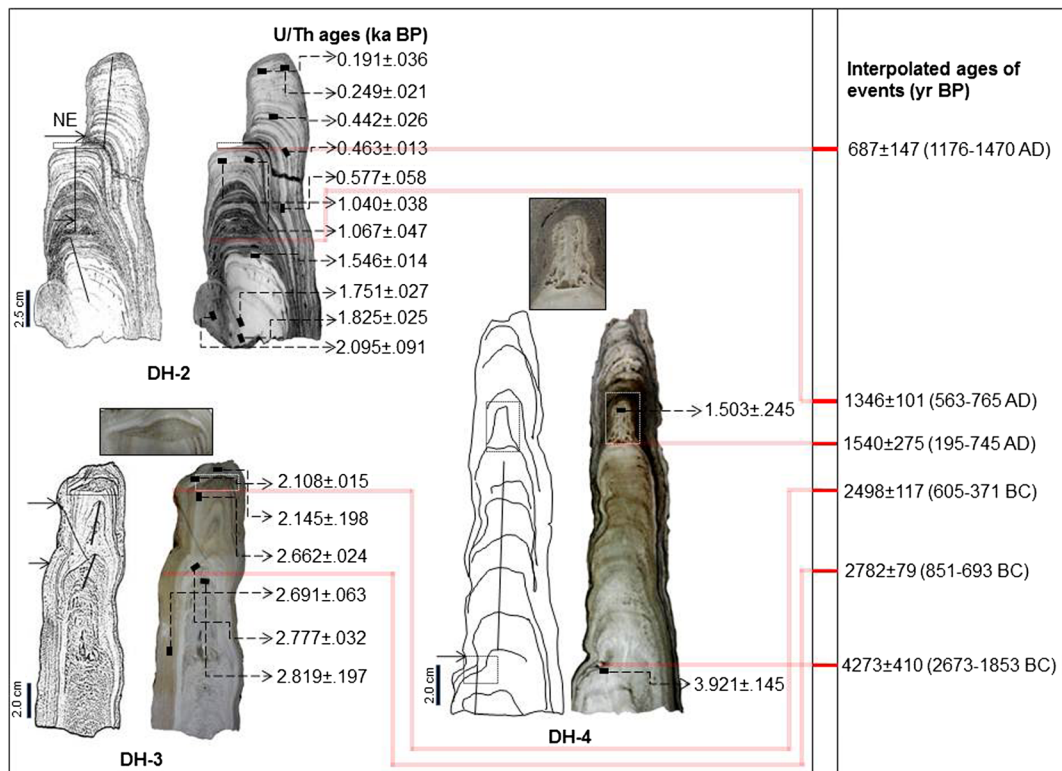


Fig. 4 Polished vertical sections of stalagmites (DH-2, DH-3, and DH-4) with graphical replicas showing growth layers anomalies and U-Th ages (see also Table 1). Numbers on the right side denote interpolated ages, and black vertical lines within the graphical representations denote the changes in growth axes; the arrows on

the left side indicate the direction of tilt. The close-ups of growth anomalies within DH-3 and DH-4 of the corresponding areas shown in respective boxes on the top of the polished sections (see also Table 2)

uniformly distributed from bottom to top as compared to six dates from DH-3 and two dates from DH-4. For the last two samples, the presence of impurities (thorium contamination) in the stalagmites compelled us to avoid those depths, and therefore, the dates on these samples are not adequately distributed throughout their lengths (Fig. 4). We have calculated the growth rate of DH-3 based on the available data (six dates), but DH-4 could not be included with only two dates (Fig. 5).

6 Discussion and conclusions

We have used changes in the orientation of the growth axis and breakage of stalagmites as potential proxies for seismic events. The deformation features identified in each stalagmite sample can be explained by earthquake-induced events such as tilting of the cave floor or a shift in the position of drip water relative to the sample due to a change in the alignment of the ceiling. The sample

DH-2 shows a major tilt in the vertical growth axis toward northeast (Fig. 4). The shift is explained as due to movement of drip location that could be possibly associated with earthquake-induced ground shaking. An alternate mechanism may include shifting of fractures driven by local slope instability that induces closure of active dripping roof fractures and generation of new adjacent ones (Becker et al. 2006). The shifts in the growth axis may also be caused by fracture dormancy induced by pervasive drought succeeded by a wet period. However, the oxygen isotope analyses of this specimen in a previous independent study at these depth levels are not suggestive of any abrupt variability in climatic conditions (e.g., Sanwal et al. 2013). Further, the younger shift at the upper level seems to be abrupt, generally consistent with a seismic event.

A younger event 687 ± 147 years BP (1176–1470 AD) obtained from DH-2 is somewhat correlative with the ages (1259–1433 AD and 1050–1250 AD) of ancient earthquakes ($M_w \geq 8.0$) obtained

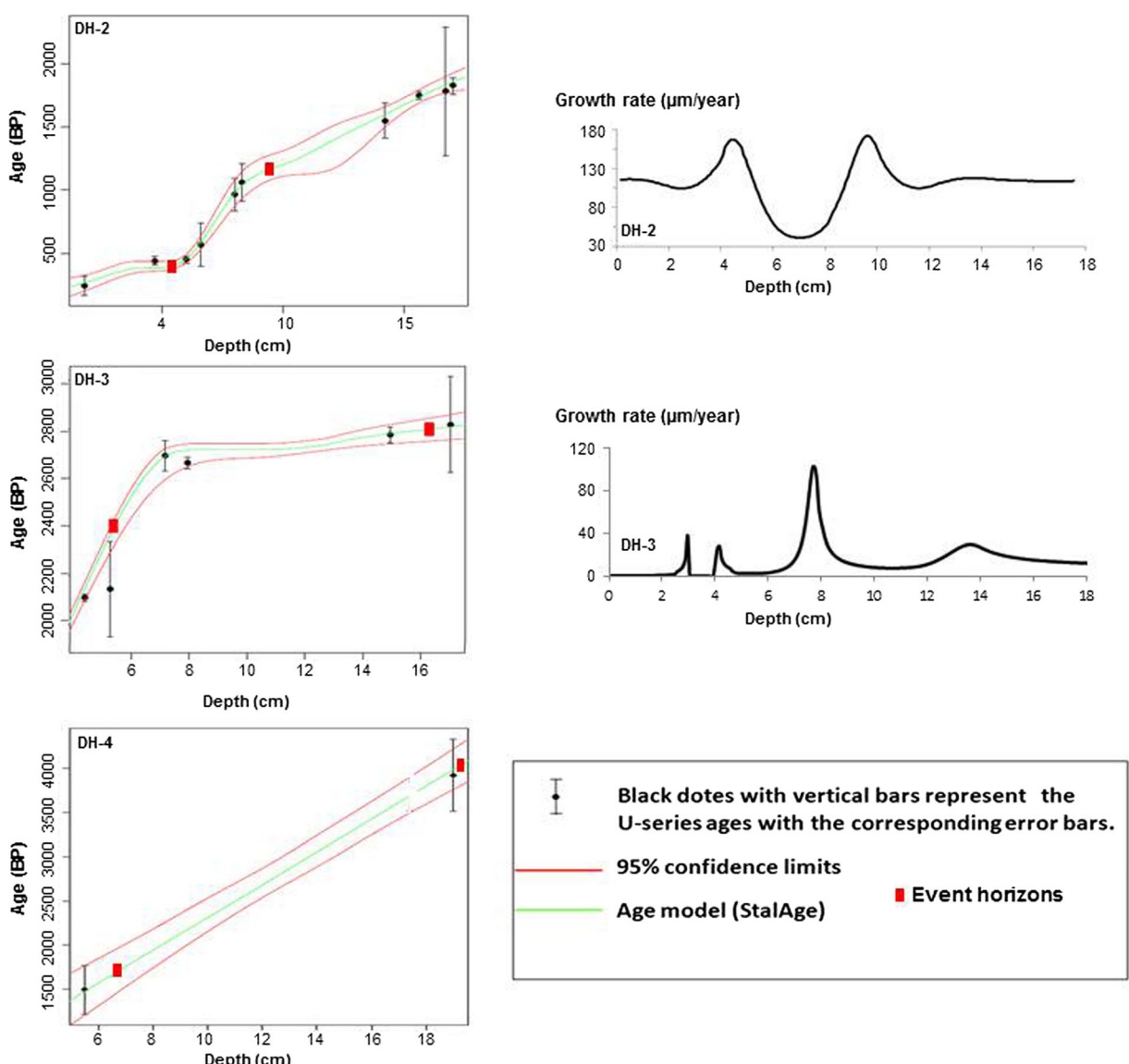


Fig. 5 Graphs showing interpolated dates of stalagmite growth layers based on the StalAge algorithm for the samples DH-2, DH-3, and DH-4 (age-depth models, following Scholz and Hoffmann 2011). Stalagmites DH-2 and DH-4 were in growing stage at the

time of collection, and therefore, the ages at the top of these samples are considered as zero. The graphs on the right side show growth rates ($\mu\text{m}/\text{year}$) of DH-2 and DH-3 (except DH-4, for lack of sufficient age data)

from trenches across the frontal fault in the central Himalaya (Rajendran et al. 2015), located ~100 km to the south (Fig. 6). In the same sample, at the mid-level, an older generation tilt is recorded, which is dated at 1346 ± 101 years BP (563–765 AD). Much older perturbation events are also evident on DH-3 at 2782 ± 79 years BP (851–693 BC) and 2498 ± 117 years BP (605–371 BC). The breakage evident in DH-3 at ~1.5-cm depth (2498 ± 117 years BP) could be indicative of strong co-seismic shaking and eventual

damage. This stalagmite also exhibits subsequent rejuvenation as it shows indications of regrowth, while the dripping point remained stationary. As the cave floor in the Dharamjali Cave is a part of the original limestone formation and it shows no evidence of soft clay or gravel substratum, we rule out nontectonic factors. As no archaeological record of early human habitation (~2000 years ago) has been discovered in the cave, we rule out any human-induced damage. Further, the samples are collected from a narrow chamber, located far

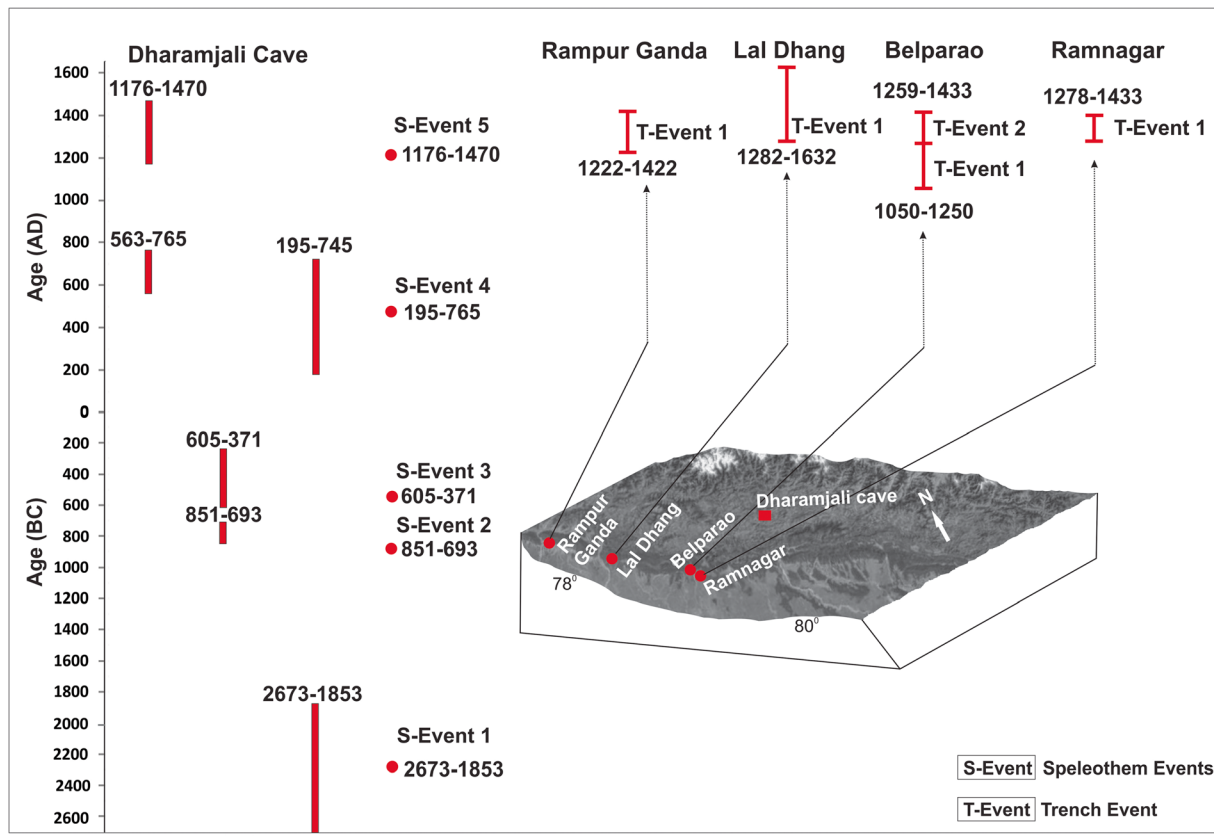


Fig. 6 Interpolated ages (based on StalAge) of the growth anomalies (*bars in red*) from stalagmites and dates of paleoearthquakes (dates marked as “S” and “T” to differentiate between speleothems and trenches, respectively). The previous fault excavation sites along the frontal thrust: Ramnagar (Kumar et al. 2006); Belparao

(Rajendran et al. 2015); Lal Dhang (Kumar et al. 2006); and Rampur Ganda (Kumar et al. 2006); age ranges (vertical bars) of earthquakes from corresponding trench sites are shown on the right side

from the habitable part (for humans or other primates/mammals) of the cave (Fig. 4).

The stalagmite DH-4 showcases an embedded broken soda straw or stalactite at a depth of ~7.8 cm, followed by upward growth (Fig. 4). This feature is indicative of a scenario in which the stalagmite grew, gaining in height until eventually merging with a soda straw on the roof at which point it was broken. When the soda straw broke, possibly during an earthquake, it must have remained attached to the intact stalagmite growing from below and the continuing processes of dripping and precipitation allowed it to become embedded within newer growth layers. The date of the breakage event is constrained by the U-Th date of the piece of soda straw (1503 ± 245 years BP; 262–752 AD) entrapped within the stalagmite. A transitional zone from lighter colored growth bands to darker shades can be detected at almost same period (1546 ± 014 years BP) at the lower part of

DH-2. It should also be mentioned here that a closely similar date (1590 ± 240 years) is registered at the zone of a major growth axis tilt on a stalagmite specimen from “Siddha Baba” Cave ($27^{\circ} 59' N, 84^{\circ} 04' E$; 2000 m msl) in central Nepal, about 500 km, east of Pithoragarh, the location of Dharamjali Cave (see Denniston et al. 2000). A possible explanation for this simultaneity in deformation is that the causative earthquake probably had ruptured long enough to impact the two caves.

An important point is the threshold shaking intensity required to deform or damage the modern speleothems in limestone caves. Although no contemporary reports are available on damage to the Himalayan caves due to earthquakes, observations recorded from Japan, France, and Bulgaria provide a few pointers. For example, cave collapse and severe damage has been reported from a cave in Bulgaria during the 1928 Ms 7.0 Chirpan

earthquake located about 55 km southwest of the epicenter (Becker et al. 2006). A counter example is the 1995 Ms 7.2 Kobe (Japan) earthquake as the post-earthquake observations did not reveal any damage to the near source caves (Gilli and Delange 2001). Further, even in caves that showed earthquake damages (e.g., a near source moderate 1996 St.-Paul-de-Fenouillet earthquake in France), the percentage of “damaged to undamaged speleothems” (mostly restricted to soda straws) was generally very small (less than 20 %) and only the “most elevated” cave at an altitude of 840 m showed any significant damage (Gilli 1999).

The shaking intensity required to damage speleothems, as shown by a few previous examples, suggest an intensity exceeding VII on the Medvedev-Sponheuer-Karnik scale, equivalent to a magnitude >5.0, if the earthquake was originated very close to the cave (Gilli 1999). At the Dead Sea Transform region, it is suggested that accelerations in excess of 1 g, which generally result from events of M 7.5–8.0 at a distance of ~60 km, would be required to break speleothems (Kagan et al. 2005). Experimental and modeling studies, which include static and dynamic bending tests on stalagmites, also suggest high accelerations (>1 g) that are required to break these types of aragonite/calcitic depositions (Cadorin et al. 2001). These studies indicate that sufficiently long and slender speleothems, with fundamental natural frequencies within the frequency range of seismic excitations, as well as those speleothems with any structural/material weakness are vulnerable to breaking due to seismic shaking (Szeidovitz et al. 2008).

Samples DH-3 and DH-4 show evidence of breakage and regrowth; the former showing regrowth after breakage, while the latter preserves evidence of a broken straw. Using the same tensile stress and density values after Cadorin et al. (2001), the critical horizontal ground acceleration required to break the Dharamjali stalagmites at the bottom part of them in static case would be much higher than 1 g, although these values may change (e.g., Szeidovitz et al. 2008). If high ground acceleration is an acceptable scenario for the growth deformation recorded in the Dharamjali Cave, it is likely that these were produced by proximal extreme events and consequent ground level changes. It is equally possible that the damage registered on the Dharamjali Cave could have resulted from major earthquakes on the hinterland faults in the vicinity of the cave that may not have ruptured the surface. The above premise should

have been applicable to the historically documented 1803 earthquake ($M \sim 7.5$), located ~70 km west of Dharamjali Cave (Fig. 1a). This earthquake should have ideally generated damage at the cave site. Our data show that the 1803 earthquake has apparently left no imprints of deformation on DH-2, which is the only sample that spans this time period. It is worth noting that the damage pattern observed on the ancient monuments (temples) of the same period and the impact of this earthquake on regional structures has not been uniform (Rajendran et al. 2013).

We also have to take into account of the fact the seismic waves tend to attenuate with depth (e.g., Becker et al. 2006). However, the Dharamjali Cave occurs under a shallow depth of limestone formation (30–50 m), and consequently the attenuation factor of seismic waves for horizontal components is expected to be very low (~20 %) (e.g., Gribovszki et al. 2013). Thus, for the reasons why the 1803 earthquake did not have much impact on this cave we may have to look at other possibilities. The amplification effect also depends on a complex combination of nature of geological material (e.g., length, width, and overall strength of stalagmites) and various spatial/geometrical considerations along with azimuth, distance, and size of the seismic events (Geli et al. 1988). Although our sample (DH-2) does not show deformation due to the 1803 earthquake, the future studies could focus on the floor debris to identify any collapse of the cave roof or soda straws that can be attributed to this historical earthquake. One assumption is that growth anomalies of the samples presented here can only be generated by proximal great earthquakes ($M \geq 8.0$), but this remains a conjecture until more samples can be acquired across a larger area.

The deformations within the stalagmites in this study, if indeed they represent major earthquakes suggest variable interval between successive events at a first approximation. Our present results are inconclusive as they are restricted to a single cave in the central Himalaya. The unavailability of a statistically reasonable number of deformed samples for comparison places limitations on our ability to reach definitive conclusions on recurrence pattern of earthquakes in the Uttarakhand Himalaya. Sampling additional caves may bring further clarity on different modes of speleothem damage and their recurrence. In the meantime, the cave records presented here will remain as a template for future speleoseismite studies aimed at quantifying longer-term earthquake time series in the Himalaya.

Acknowledgments This work was funded by the Australia-India Strategic Research Fund. JS was supported by the fast track scheme under the Department of Science and Technology, Govt. of India (No. SR/FTP/TS-97/2009) and BSK by AvH Linkage Project (No. 3-4-FoKoop, 396 DEU/1017420) and Ministry of Earth Sciences, New Delhi. JS and CPR thank Tribhuvan Singh (Pithoragarh) for his assistance during multiple visits to the study site for sampling. This paper has improved considerably after thorough reviews by Katalin Gribovszki and Elisa Kagan, and we are grateful to both of them for their time, patience, and efforts.

References

- Ambraseys N, Jackson D (2003) A note on early earthquakes in northern India and southern Tibet. *Curr Sci* 84:571–582
- Atkinson TC, Harmon RS, Smart PL, Waltham AC (1978) Palaeoclimate and geomorphic implications of $^{230}\text{Th}/^{234}\text{U}$ dates on speleothems from Britain. *Nature* 272:24–28
- Baker A, Smart PL, Ford DC (1993a) Northwest European paleoclimate as indicated by growth frequency variations of secondary calcite deposits. *Palaeogeogr Palaeoclimatol Palaeoecol* 100:291–301
- Baker A, Smart PL, Edwards RL, Richards DA (1993b) Annual growth banding in a cave stalagmite. *Nature* 364:518–520
- Banner JL, Guilfoyle A, James EW, Stern LA, Musgrove M (2007) Seasonal variations in modern speleothem calcite growth in Central Texas, USA. *Int J Sediment Res* 77:615–622. doi:[10.2110/2007.065](https://doi.org/10.2110/2007.065)
- Becker A, Davenport CA, Eichenberger U, Gilli E, Jeannin PY, Lacave C (2006) Speleoseismology: a critical perspective. *J Seismol* 10:371–388
- Bilham R, Ambraseys N (2005) Apparent Himalayan slip deficit from the summation of seismic moments for Himalayan earthquakes, 1500–2000. *Curr Sci* 88:1658–1663
- Braun Y, Kagan E, Bar-Matthews M, Ayalon A, Agnon A (2011) Dating speleoseismites near the Dead Sea Transform and the Carmel Fault: clues to coupling of a plate boundary and its branch. *Isr J Earth Sci* 58:257–273
- Cadorin JF, Jongmans D, Plumier A, Camelbeeck T, Delaby S, Quinif Y (2001) Modelling of speleothems failure in the Hottot Cave (Belgium). Is the failure earthquake induced? *Neth J Geosci* 80:315–321
- Célérier J, Harrison TM, Webb AAG, Yin A (2009) The Kumaun and Garwhal Lesser Himalaya, India: Part 1. Structure and stratigraph. *Geol Soc Am Bull* 121:1262–1280. doi:[10.1130/B263441](https://doi.org/10.1130/B263441)
- Cheng H, Lawrence Edwards R, Shen CC, Polyak VJ, Asmerom Y, Woodhead JD, Hellstrom J, Wang Y, Kong X, Spötl C, Wang X, Calvin Alexander E Jr (2013) Improvements in ^{230}Th dating, ^{230}Th and ^{234}U half-life values, and U–Th isotopic measurements by multi-collector inductively coupled plasma mass spectrometry. *Earth Planet Sci Lett* 371–372:82–91
- Delaby S (2001) Palaeoseismic investigations in Belgian caves: Netherlands. *J Geogr Sci* 80:323–332
- Denniston RF, González LA, Asmerom Y, Sharma RH, Reagan MK (2000) Speleothem evidence for changes in Indian summer monsoon precipitation over the last ~2300 years. *Quat Res* 53:196–202
- Dorale JA, Edwards RL, Ito E, Gonzalez IE (1998) Climate and vegetation history of the midcontinent from 75 to 25 ka: A speleothem record from Crevice Cave, Missouri, USA. *Science* 282:1871–1874
- Duan W, Kotlia BS, Tan M (2013) Mineral composition and structure of the stalagmite laminae from Chulerasim cave, Indian Himalaya and the significance for palaeoclimatic reconstruction. *Quat Int* 298:93–97
- Fairchild IJ, Baker A (2012) *Speleothem Science*. Wiley, Chichester, p 432
- Fleitmann D, Burns SJ, Neff U, Mudelsee M, Mangini A, Matter A (2004) Palaeoclimatic interpretation of high-resolution oxygen isotope profiles derived from annually laminated speleothems from Southern Oman. *Quat Sci Rev* 23:935–945
- Forti P (2001) Seismotectonic and paleoseismic studies from speleothems: the state of the art: Netherlands. *J Geosci* 80: 175–185
- Forti P, Postpischl D (1984) Seismotectonic and paleoseismic analyses using karst sediments. *Mar Geol* 55:145–161
- Geli L, Bard PJ, Julien B (1988) The effect of topography on earthquake ground motion: a review and new results. *Bull Seismol Soc Am* 78:42–63
- Gilli E (1999) Evidence of paleoseismicity in a flowstone of the Observatoire cave (Monaco). *Geodin Acta* 12:159–168
- Gilli E (2004) Glacial causes of damage and difficulties to use speleothems as palaeoseismic indicators. *Geodin Acta* 17: 229–240
- Gilli E (2005) Review on the use of natural cave speleothems as palaeoseismic or neotectonics indicators. *Compt Rendus Geosci* 337:1208–1215
- Gilli E, Delange P (2001) Utilisation des speleothèmes comme indicateurs de neotectonique oude la paleoseismite. In: Gilli E, Audra P (eds) *Tectonique Active et Geomorphologie, Revd'Analyse Spatiale Quantitative et Appliquee*, Spec. Publ: 79–90
- Gopher A, Ayalon A, Bar-Matthews M, Barkai R, Frumkin A, Karkanas P, Shahack Gross R (2010) The chronology of the late Lower Paleolithic in the Levant based on U/Th ages of speleothems from Qesem Cave, Israel. *Quat Geochronol* 5: 644–656
- Gribovszki K, Kovács K, Mónus P, Shen C-C, Török Á, Brimich L (2013) Estimation of an upper limit on prehistoric peak ground acceleration using the parameters of intact stalagmites and the mechanical properties of broken stalagmites in Domica cave, Slovakia, Slovensky kras (ACTA Carsologica Slovaca 51(1–2):5–14
- Hellstrom J (2003) Rapid and accurate U/Th dating using parallel ion counting multi-collector ICP-MS. *J Anal At Spectrom* 18:1346–1351
- Hellstrom J (2006) U-Th dating of speleothems with high initial ^{230}Th using stratigraphical constraints. *Quat Geochronol* 1: 289–295
- Holzkämper S, Holmgren K, Lee-Thorp J, Talma A, Mangini A, Partridge T (2009) Late Pleistocene stalagmite growth in Wolberg Cave, South Africa. *Earth Planet Sci Lett* 282: 212–221. doi:[10.1016/j.epsl/2009.03.016](https://doi.org/10.1016/j.epsl/2009.03.016)
- Kagan EJ, Agnon A, Bar-Matthews M, Ayalon A (2005) Dating large infrequent earthquakes by damaged cave deposits. *Geology* 33:261–264

- Khattri KN (1987) Great earthquakes, seismicity gaps and potential for earthquake disaster along the Himalaya plate boundary. *Tectonophysics* 138:79–92
- Kotlia BS, Ahmad SM, Zhao JX, Raza WK, Collerson D, Joshi LM, Sanwal J (2012) Climatic fluctuations during the LIA and post-LIA in the Kumaun Lesser Himalaya, India: evidence from a 400 yr old stalagmite record. *Quat Int* 263:129–138
- Kotlia BS, Singh AK, Joshi LM, Dhaila BS (2014) Precipitation variability in the Indian Central Himalaya during last ca. 4, 000 years inferred from a speleothem record: Impact of Indian Summer Monsoon (ISM) and Westerlies. *Quat Internat.* doi:[10.1016/j.quaint/201410066](https://doi.org/10.1016/j.quaint/201410066)
- Kumar S, Wesnousky S, Rockwell TK, Briggs RW, Thakur VC, Jayangondaperumal R (2006) Paleoseismic evidence of great surface rupture earthquakes along the Indian Himalaya. *J Geophys Res* 111, B03304. doi:[10.1029/2004JB003309](https://doi.org/10.1029/2004JB003309)
- Kumar S, Wesnousky S, Jayangondaperumal R, Nakata T, Kumahara Y, Singh V (2010) Paleoseismological evidence of surface faulting along the northeastern Himalayan front, India: timing, size, and spatial extent of great earthquakes. *J Geophys Res* 115, B12422. doi:[10.1029/2009JB006789](https://doi.org/10.1029/2009JB006789)
- Lemeille F, Cushing M, Carbon D, Grellet B, Bitterli T, Flehocand C, Innocent C (1999) Co-seismic ruptures and deformations recorded by speleothems in the epicentral zone of the Basel earthquake. *Geol Acta* 12:179–191
- Mahesh P, Rai SS, Sivaram K, Paul A, Gupta S, Sarma R, Gaur VK (2013) One dimensional reference velocity model and precise locations of earthquake hypocenters in the Kumaon-Garhwal Himalaya. *Bull Seismol Soc Am* 103:328–339. doi:[10.1785/0120110328](https://doi.org/10.1785/0120110328)
- Mariethoz G, Kelly BFJ, Baker A (2012) Quantifying the value of laminated stalagmites for paleoclimate reconstructions. *Geophys Res Lett* 39, L05407. doi:[10.1029/2012GL050986](https://doi.org/10.1029/2012GL050986)
- Morell KD, Sandiford M, Rajendran CP, Rajendran K, Alimanovic A, Fink D, Sanwal J (2015) Geomorphology reveals active décollement geometry in the central Himalayan seismic gap. *Lithosphere*. doi:[10.1130/L407.1](https://doi.org/10.1130/L407.1)
- Musgrove ML, Banner JL, Mack LE, Combs DM, James EW, Cheng H, Edwards RL (2001) Geochronology of late Pleistocene to Holocene speleothems from central Texas: Implications for regional paleoclimate. *Geol Soc Am Bull* 113(12):1532–1543
- Ni J, Barazangi M (1984) Seismotectonics of the Himalayan collision zone: geometry of the underthrusting Indian plate beneath the Himalaya. *J Geophys Res* 80:1142–1163
- Orlando IJ, Bar-Matthews M, Ayalon A, Matthews A, Kozdon R, Ushikubo T, Valley JW (2012) Seasonal resolution of Eastern Mediterranean climate change since 34 ka from a Soreq Cave speleothem. *Geochim Cosmochim Acta* 89:240–255
- Pandey MR, Tandukar RP, Avouac JP, Lave' J, Massot JP (1995) Interseismic strain accumulation on the Himalayan crustal ramp (Nepal). *Geophys Res Lett* 22:751–754
- Panno SV, Craig CL, Hackley KC, Curry BB, Fouke BW, Zhang Z (2009) Major earthquakes recorded by speleothems in mid-western U.S. caves. *Bull Seismol Soc Am* 99:2147–2154. doi:[10.1785/0120080261](https://doi.org/10.1785/0120080261)
- Parameswaran R, Thulasiraman N, Rajendran K, Rajendran CP, Mullick R, Wood M, Lekhak H (2015) Seismotectonics of the April-May 2015 Nepal earthquakes: An assessment based on the aftershock patterns, surface effects and deformation characteristics. *Asian J Earth Sci.* doi:[10.1016/j.jseaes.2015.07.030](https://doi.org/10.1016/j.jseaes.2015.07.030)
- Postpischl D, Agostini S, Forti P, Quinif Y (1991) Paleoseismicity from karst sediments: the “Grotta del Cervo” cave case study (Central Italy). *Tectonophysics* 193:33–44
- Railsback LB, Pete DA, Lixin W, Genevieve A, Holdridge NRV (2013) Layer-bounding surfaces in stalagmites as keys to better paleoclimatological histories and chronologies. *Int J Speleol* 42:167–180
- Rajendran CP, Rajendran K (2011) Revisiting some significant earthquake sources in the Himalaya: Perspectives on past seismicity. *Tectonophysics* 504:75–88
- Rajendran CP, Rajendran K, Sanwal J, Sandiford M (2013) Archeological and historical database on the medieval earthquakes of the central Himalaya: Ambiguities and inferences. *Seismol Res Lett* 87:1098–1108
- Rajendran CP, John B, Rajendran K (2015) Medieval pulse of great earthquakes in the central Himalaya: Viewing past activities on the frontal thrust. *J Geophys Res* 120:1623–1641. doi:[10.1002/2014JB011015](https://doi.org/10.1002/2014JB011015)
- Sanwal J, Kotlia BS, Rajendran CP, Masood SA, Rajendran K, Sandiford M (2013) Climatic variability in Central Indian Himalaya for the last ~1,800 years: Evidence from high-resolution speleothem record. *Quat Int* 304:183–192
- Sapkota SN, Bollinger L, Klinger Y, Tappognon P, Gaudemer Y, Tiwari D (2013) Primary surface ruptures of the great Himalayan earthquakes in 1934 and 1255. *Nat Geosci* 6: 71–76. doi:[10.1038/ngeo1669](https://doi.org/10.1038/ngeo1669)
- Scholz D, Hoffmann DL (2011) StalAge—an algorithm designed for construction of speleothem age models. *Quat Geochronol* 6:369–382
- Scholz D, Hoffmann DL, Hellstrom J, BronkRamsey C (2012) A comparison of different methods for speleothem age modelling. *Quat Geochronol* 14:94–104
- Šebela S (2008) Broken speleothems as indicators of tectonic movements. *Acta Cardiol* 37:51–62
- Shen CC, Wu CC, Cheng H, Edwards RL, Hsieh YT, Gallet S, Chang CC, Li TY, Lam DD, Kano A, Hori M, Spötl C (2012) High-precision and high-resolution carbonate 230Th dating by MC-ICP-MS with SEM protocols. *Geochim Cosmochim Acta* 99:71–86. doi:[10.1016/j.gca.2012.09.018](https://doi.org/10.1016/j.gca.2012.09.018)
- Shen CC, Lin K, Duan W, Jiang Z, Partin JW, Edwards LR, Cheng H, Tan M (2013) Testing the annual nature of speleothem banding. *Sci Rep* 3:2633. doi:[10.1038/srep02633](https://doi.org/10.1038/srep02633)
- Shopov YY, Ford DC, Schwarzc HP (1994) Luminescent microbanding in speleothems: High-resolution chronology and paleoclimate. *Geology* 22:407–410
- Sinha A, Cannariato KG, Stott LD, Li HC, You CF, Cheng H, Edwards RL, Singh IB (2005) Variability of Southwest Indian summer monsoon precipitation during the Bølling-Allerød. *Geology* 33:813–816
- Szeidovitz G, Surányi G, Gribovszki K, Bus Z, Leél-Ossy S, Varga Z (2008) Estimation of an upper limit on prehistoric peak ground acceleration using the parameters of intact speleothems in Hungarian caves. *J Seismol* 12:21–33. doi:[10.1007/s.10950.007.9068.9](https://doi.org/10.1007/s.10950.007.9068.9)
- Treble PC, Chappell J, Shelley JMG (2005) Complex speleothem growth processes revealed by trace element mapping and scanning electron microscopy of annual layers. *Geochim Cosmochim Acta* 69:4855–4863

- Vaks A, Bar-Matthews M, Ayalon A, Matthews A, Frumkin A, Dayan U, Halicz L, Almogi-Labin A, Schilman B (2006) Paleoclimate and location of the border between Mediterranean climate region and the Saharo–Arabian Desert as revealed by speleothems from the northern Negev Desert, Israel. *Earth Planet Sci Lett* 249:384–399. doi:[10.1016/j.epsl.2006.07.009](https://doi.org/10.1016/j.epsl.2006.07.009)
- Vaks A, Gutareva OS, Breitenbach SFM, Avirmed E, Mason AJ, Thomas AL, Osinzev AV, Kononov AM, Henderson GM (2013) Speleothems Reveal 500,000-Year History of Siberian Permafrost. *Science* 340:183–186
- Valdiya KS (1980) Geology of Kumaun Lesser Himalaya. Wadia Institute of Himalayan Geology, Dehradun, p 294p
- Valdiya KS (2010) The making of India – Geodynamic evolution. Macmillan Publishers India Ltd., India, p 816p
- Wobus CW, Whipple KX, Hodges KV (2006) Neotectonics of the Central Nepalese Himalaya: constraints from geomorphology, detrital $^{40}\text{Ar}/^{39}\text{Ar}$ thermochronology and thermal modelling. *Tectonics* 25:4011. doi:[10.1029/2005TC001935](https://doi.org/10.1029/2005TC001935)